Available online at www.sciencedirect.com

SCIENCE DIRECT®

ELSEVIER

Thin Solid Films 489 (2005) 63 – 67

thin solid films

www.elsevier.com/locate/tsf

# Complexity of the microstructure evolution for optimization cBN growth in a four-step ion-assisted deposition process

S.F. Wong[a,*], C.W. Ong[a], G.K.H. Pang[a], Q. Li[b], W.M. Lau[b]

[a]Department of Applied Physics and Materials Research Centre, The Hong Kong Polytechnic University, Kowloon, Hong Kong, PRC
[b]Department of Physics, The Chinese University of Hong Kong, Shatin, New Territory, Hong Kong, PRC

Received 4 June 2004; received in revised form 7 February 2005; accepted 29 April 2005
Available online 27 June 2005

**Abstract**

The changes in microstructure of a specially prepared boron nitride (BN) film as a function of film depth were studied by high resolution transmission electron microscopy (HRTEM) and other materials analysis tools. These changes were then correlated to the changes in processing parameters during film growth. The analyzed film was fabricated by the four-step ion-assisted deposition procedure known to be effective in film-stress engineering for the formation and retention of a thick cubic BN (cBN) layer with a three-step buffer-layer deposition. In this deposition, the energy of the ions assisting cBN formation was increased stepwise from 200 to 280, and then to 360 eV [S.F. Wong, C. W. Ong, G.K.H. Pang, K.Z. Baba-Kishi, W. M. Lau, J. Vac. Sci. Technol. A 22 (2004) 676]. The nominal thickness of the cBN layer was 650 nm and that for each of the three buffer layers was about 160 nm. Both the HRTEM and electron diffraction results confirmed that the top cBN layer, with a thickness of 643 nm, consisted of cBN grains with a preferred orientation of their *c*-axis along the film growth direction. In comparison, the three-step buffer layer deposition yielded complex and intriguing microstructures. In the first buffer layer adjacent to the substrate, grains containing $sp^2$ planes with a preferred orientation of their basal planes parallel to the film growth direction were the main constituents. The increase of ion energy from 200 to 280 eV for the formation of the second buffer layer first led to an enrichment of the concentration of these $sp^2$ grains with the preferred orientation. Then, bending of some of the $sp^2$ planes into curved microstructures was evident. The microstructure became very complex and displayed multiple phases including some amorphous structures. The presence of a cBN-like phase was indeed detected by electron energy loss spectroscopy. This complex microstructure persisted until it was replaced by the cBN structure, without abrupt change when the ion energy was increased from 280 to 360 eV for the deposition of the third buffer layer. It is proposed that small grains with cBN-like $sp^3$ bonding configurations are present in the 2nd and 3rd buffer layers, probably with crystalline domains less than 5 nm and thus difficult for direct detection even by HRTEM. A sufficient accumulation of these cBN nuclei transformed the buffer layer to the cBN layer.
© 2005 Elsevier B.V. All rights reserved.

*Keywords:* Boron nitride; Growth mechanism; Structural properties; Transmission electron microscopy (TEM)

## 1. Introduction

Boron nitride (BN) films with a high cubic BN (cBN) content have excellent mechanical properties and promise great applications in surface coating technology [2–5]. It is now widely accepted that cBN-rich films can be synthesized under ion bombardment with energy ($U_{assist}$) exceeding a certain threshold value. It is also widely accepted that even in a single-step process (where $U_{assist}$ and other deposition parameters were kept constant), the film deposited still exhibits a layered structure. Such a layered structure typically consists of a thin disordered layer (aBN) on the substrate surface, then a layer having randomly packed $sp^2$-bonded graphite-like planes (often referred as turbostratic BN, tBN), and finally a cBN-rich top layer [6 7]. Different theories, like the static stress model [8,9], dynamic stress model [5], subplantation model [10], quenching model [11] and sputter model [7], have been proposed to describe the

* Corresponding author.
*E-mail address:* 96586087.sf@polyu.edu.hk (S.F. Wong).

0040-6090/$ - see front matter © 2005 Elsevier B.V. All rights reserved.
doi:10.1016/j.tsf.2005.04.118

evolution and growth mechanisms of the cBN phase. A more recent report on ab initio calculations of free energies of various BN phases and studies of their phase transformation further articulate the effects of film stress on the compression of the graphite-like hexagonal BN to the dense and hard wurtzitic BN (the soft rhombohedral BN to the hard cBN). It also explains that defects in these crystalline phases can raise their free energies and thereby facilitate the relevant phase transformation and nucleation during BN film growth [12]. On the whole, the growth mechanisms for various BN phase formations in all known BN film deposition processes are rather complex because different mechanisms may take place at different stages in a BN film deposition process and variations in deposition design can also invoke different mechanisms. The evolution sequence for the mechanisms to take place will be affected by the changes in deposition conditions (e.g. $U_{assist}$, ion species and their current densities, and growth temperature) during film growth. On the other hand, it will also be reflected by some resultant structural changes as a function of film depth. The extension of research in both experimental studies of microstructure evolution as a function of deposition attributes and theoretical examinations of relevant growth mechanisms are certainly synergetic.

This synergy is shown in a BN film deposition process disclosed recently, a process which was designed by following the theoretical guideline of stress-induced cBN formation and the experimental experience in practical film stress evolution and control. This led to the successful formation and retention of a thick cBN film by adopting a four-step approach (referred as the four-step BN film deposition thereinafter) [1]. In this process, the first three steps comprise of a typical ion-assisted BN deposition procedure at an optimal and constant substrate temperature (680 °C), and a stepwise increase in $U_{assist}$ from 200, 280 and 360 eV for the deposition of a BN film of ~160 nm in each step. This three-step process is known to build up a buffer layer with a gradual increase in film stress [1]. Although the conventional Fourier transform infrared absorption (FTIR) measurements on such buffer films do not show any detectable cBN content, a cBN-rich layer can be formed virtually on top of this buffer layer when $U_{assist}$ is changed to 450 eV. More importantly, the three-step buffer layer deposition also accommodates the formation and retention of a cBN-rich layer of over 500 nm in thickness, whereas a cBN-rich layer of more than 100 nm peels off from the substrate without the buffer layer deposition [1]. The success in this process optimization to improve the cBN film deposition results calls for detailed studies of the associated microstructure evolution, such that further theoretical studies and experimental process optimization can be conducted.

The present article reports on the complex microstructures and their evolutions in the BN film prepared by the four-step BN film deposition. The microstructure data were collected from high resolution transmission electron microscopy (HRTEM), selected area electron diffraction analysis (SAED), FTIR, and electron energy loss spectroscopy (EELS).

## 2. Experimental methods

The film sample was deposited on Si (100) substrate at 680 °C by using a high vacuum system equipped with two 3-cm Kaufman ion guns (Ion Tech, Inc.) [13]. Boron was sputtered from a 4-in. B target (99.9%) by an argon ion ($Ar^+$) beam of 70 mA and 1200 eV generated by one ion gun. The substrate was bombarded simultaneously by an $Ar^+/N_2^+$ ion beam generated by another ion gun. The flow rates of the Ar and $N_2$ gases admitted into the second ion gun were in a ratio of 1.2:1. The four-step BN film deposition began with a three-step buffer layer deposition, $U_{assist}$ increased stepwise from 200 to 280, and then to 360 eV. Each setting lasted for 20 min, and the beam current ($I_{assist}$) was kept constant at 20 mA. After the buffer layer deposition process, a cBN-rich layer was deposited, with $U_{assist}$ and $I_{assist}$ set at 450 eV and 30 mA respectively. This step lasted for 180 min.

Cross-sectional transition electron microscopy (TEM) analysis and SAED were conducted by using a JEOL 2010 system (200 keV) and a JEOL 3000 FEG-TEM system (300 keV). The electron beam size was set to have diameters in the range of 2–100 nm. The energy resolution was around 1 eV. Results of FTIR analysis were used to estimate the volume fraction of the cBN content ($\eta_{cBN}$) in each layer according to the conventional method [14] and a Nicolet Magna-TR™ System Model 750 was employed. In this analysis, the IR absorption spectrum of a three-layered buffer layer was collected separately from another sample prepared by following the abovementioned procedures. As such, the cBN content in the top layer is deduced by means of proper data subtraction. For the measurements of BN phase composition of the top surface layer of ~1 nm, the technique of EELS was applied, with a Quantum 2000 PHI photoelectron spectrometer [15]. The method deconvolutes the EELS data (arising from the nitrogen 1 s photoelectrons injected by an Al $K_\alpha$ X-ray source) collected from the top surface layer to a phase composition of a mixture of aBN, hBN and cBN, through a comparison of the measured data with those collected from three pure-phase standards. Finally, chemical composition measurements by X-ray photoelectron spectroscopy (XPS) were performed also with the Quantum 2000 PHI spectrometer.

## 3. Results and discussion

### *3.1. Layer structure of the BN film*

The low magnification cross-sectional TEM image of the film sample (Fig. 1) reveals a layered structure containing a

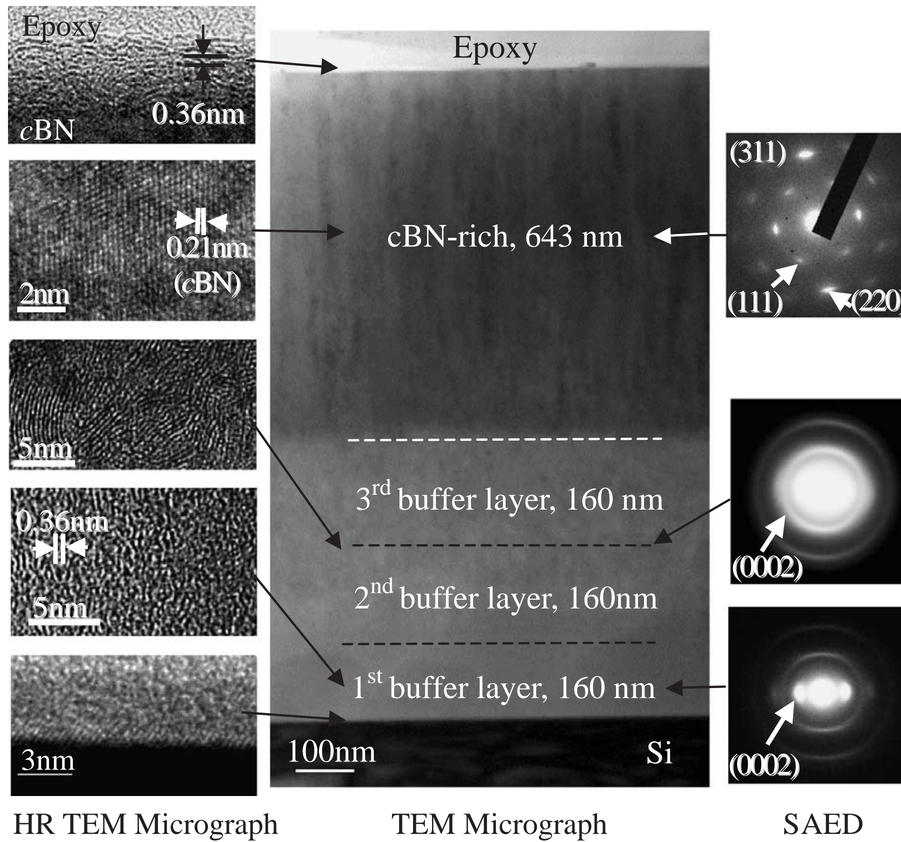


Fig. 1. Low magnification cross-sectional image; high magnification TEM images and SAED patterns of selected points at different depths of a film containing a 492-nm buffer layer and a 643-nm Cbn-rich layer.

492-nm buffer layer and a 643-nm cBN-rich top layer. The FTIR results show no cBN content at all in the buffer layer but the presence of 87% cBN in the top layer (by volume).

A dark field TEM image of the buffer layer (Fig. 2), which was obtained from the Fourier transform of a selected electron diffraction spot to reveal the structural details in the buffer layer. It decorates the location of graphite-like $sp^2$ planes aligned along the growth direction with a bright contrast. The 1st sub-buffer layer corresponds to the region deposited at $U_{assist}$ of 200 eV. The remaining region in the buffer layer was deposited at $U_{assist}$ of 280 and 360 eV. Although there is no a clearly observable boundary separating the 2nd and 3rd sub-buffer layers, we have still included a layer marker in Figs. 1 and 2 by assuming that the deposition rates were approximately the same in the two deposition steps.

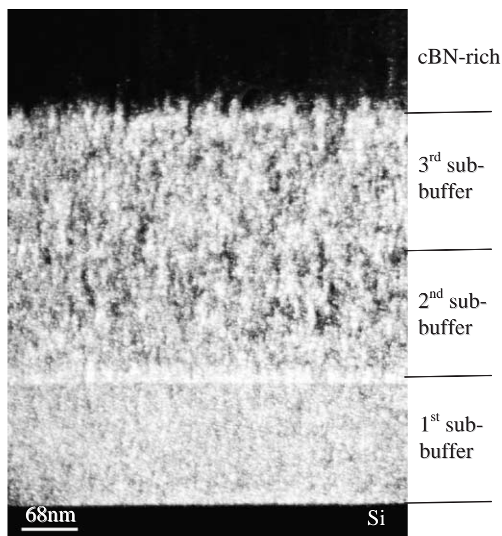


Fig. 2. Dark field image of the buffer layer. The bright areas represent $sp^2$ regions having graphitic planes perpendicular to the substrate surface.

### 3.2. Substrate–buffer layer interface

At the film–substrate interface region, HRTEM analysis shows a 3.8-nm thin region in which the arrangement of atoms is highly disordered (bottom left of Fig. 1). Similar disordered layers, which were found by many other groups, were sometimes grouped into the "aBN" phase [6,16–20]. Hofsäss et al. suggested that such a layer could be an ion mixing region containing atoms from the substrate and the film [21], which is adopted in the present study. Results of elemental compositional analysis for this type of highly disordered layers are seldom reported [22], because the analysis requires an extremely high spatial resolution which is not available by most techniques. One indirect support to the ion mixing model is that the projected range of 200 eV $Ar^+$ ions (used to initiate the 1st sub-buffer layer) into silicon is estimated to be ~2 nm according to the TRIM

simulation code (but the end of range is 2–3 times larger than the projected range). When boron and nitrogen are present on silicon, such argon ion bombardment is expected to induce ion mixing for the formation of an interfacial layer containing boron, nitrogen and silicon, with a thickness of comparable to the projected range of the argon ions. This result is fairly close to the thickness of the observed film–substrate interfacial layer.

### *3.3. Three sub-buffer layers*

In the 1st sub-buffer layer, grains parallel atomic planes separated by an average distance of 0.36 nm were found. The lattice spacing is identical to that of the (0002) planes in hexagonal BN (hBN). Since the chemical composition in this region consists of stoichiometric BN as confirmed by XPS, the dominant microstructure in this region must be hBN-like $sp^2$-bonded, in the bonding environment with a certain degree of randomness, as shown by the HRTEM image of this region in Fig. 1. The grains with well packed $sp^2$ planes do not necessarily possess the "ababab" plane stacking in the hBN structure, and are thus commonly referred as turbostratic BN (tBN). We adopt this label of tBN and use it in such a definition reference. The amorphous portions between the tBN grains can be formed, in the collision cascade during ion-assisted deposition, either by knocking off atoms from their normal lattice structure or by inserting interstitial atom. Interestingly, the tBN grains were well-aligned, with their basal planes along the growth direction. This is directly seen in the HRTEM image, and is supported by the SAED pattern where the diffraction spots are located in a horizontal line in parallel to the substrate surface (right column of Fig. 1).

Referring more carefully to the dark field image as shown in Fig. 2, one can see that there is a 20-nm thick bright region at the interface between the 1st and 2nd sub-buffer layers. This is supposed to be the location corresponding to the switching of the $U_{\mathrm{assist}}$ setting from 200 to 280 eV during deposition. The more pronounced brightness of this region is interpreted as that the basal planes of the tBN grains in this region are aligned more orderly along the substrate normal direction. First, we exclude the possibility that the orderly alignment of the planes is due to ion bombardment effect, because the penetration depth of 280-eV $Ar^+$ ions is calculated to be 2 nm, which is much smaller than the thickness of this region. An alternative explanation is as follows. We propose that a bombarding ion, after giving its kinetic $U_{\mathrm{assist}}$ to other atoms in the film, can create some stresses propagating to region farther than the penetration depth. The deformation is assumed to be elastic, and the affected region is spherical in shape with a radius $R$. The strain $\varepsilon$ is approximately equal to $r_o/R$, where $r_o$ is the radius of a atom (e.g. $r_o = 0.098$ nm for a B atom). The elastic energy density in the deformed region is $E\varepsilon^2/2$. Therefore, $(E\varepsilon^2/2)(4\pi R^3/3) \approx U_{\mathrm{assist}}$. The elastic modulus of the buffer layer was measured separately to be $E = 110$ GPa by nanoindentation tests [13]. When $U_{\mathrm{assist}} = 280$ eV, $R$ is estimated to be 20 nm, close to the thickness of the orderly aligned region between the 1st and 2nd sub-buffer layers. McCarty and Medlin proposed that under biaxial compressive stresses, the basal planes could deform plastically via slipping and kinking. Consequently, the planes were rotated so as to align perpendicular to the substrate [23]. This interpretation overcomes the difficulty encountered by the elastic-strain-energy arguments [24], where the Gibb's free energy of the $sp^2$ system is calculated to be minimum when the basal planes are aligned 45° relative to the substrate.

In the 2nd and 3rd sub-buffer layers, tBN grains were found but many basal planes appeared curved, and the grain orientations became quite random. Random orientation of the atomic planes is consistent with two observed results. First, the SAED pattern (right column of Fig. 1) consists mainly of circular diffused halos. Second, the bright regions in the dark field TEM image occupy a smaller volume fraction (Fig. 2), relative to the 1st sub-buffer layer. We note that similar curling of basal planes in BN films was also observed and reported by other groups [25–29].

Although FTIR gave no cBN contents in the entire buffer layer of 492 nm in thickness and no clear diffraction characteristics of cBN was displaced in this layer, EELS provided some additional insights in microstructure evolution in this buffer layer. In brief, EELS data collected from the buffer layer, when compared to those collected from a cBN crystal, hBN crystal, and a specially prepared aBN film, gave some clear evidence of the presence of cBN phase in the buffer layer [15], with a particularly high cBN concentration at the upper part of the 3rd sub-buffer layer [30]. We speculate that the cBN phase in the buffer layer was "hidden" in the form of defective cBN nanoclusters so small (like less than 5 nm) that they are difficult to be observed by FTIR, electron diffraction and HRTEM.

### *3.4. cBN-rich layer*

According to the data of IR absorption, the top layer formed by ion bombardment of 450 eV and 30 mA contains 87 vol.% of cBN. The HRTEM image of this layer clearly shows grains containing cBN (111) planes. The planes are mainly aligned along the growth direction. In some regions at the interface between the 3rd sub-buffer layer and this cBN-rich layer, the $sp^2$ basal planes and cBN (111) planes exhibit typical 2:3 matching. In addition, the transition from $sp^2$ to $sp^3$ structure appears to be rather abrupt. According to the stress model [7], massive nucleation of cBN can happen once the compressive stresses are accumulated to reach a certain threshold value [31].

Finally, the TEM image taken at the surface region of the top layer shows that there was a 3.3-nm thick $sp^2$ layer on the top of the cBN-rich layer. The basal planes were aligned in parallel with the film surface. If the direction of compressive stresses is mostly perpendicular to the basal

planes of $sp^2$-bonded layer, one may expect that the top $sp^2$ layer is not subjected to strong compressive stresses. Therefore, if the presence of compressive stresses along the *c*-axis of the basal planes is a necessary condition for the formation of $sp^3$ structure, it is difficult to image how the surface $sp^2$ planes can be converted into $sp^3$ planes since the compressive stresses applied to these planes in parallel with the film surface should be low. The mechanism responsible for continuous growth of cBN grains after nucleation should therefore be different from that for the nucleation. In addition, the effectiveness of the sputtering model is also suspicious because the theory is based on the argument that $sp^2$ phase is more readily sputtered by bombarding ions, the $sp^3$ phase can be retained. This prediction contradicts with the presence of the $sp^2$ planes lying on the top surface of the film.

## 4. Conclusion

This study shows the complex nature of the deposition process of BN films. For the optimization of cBN formation, the process needs to build up a sufficient film stress. However, a buffer layer for appropriate film stress management is required to prevent the resultant cBN layer from peeling off. For the film prepared with the four-step BN film deposition, the microstructure and phase composition evolve with observable changes as the deposition proceeds. Measuring and studying these changes offer information on the dynamical changes in growth mechanisms, which in turn may give us insights in understanding the film microstructures and developing new techniques for controlling such microstructures. We believe that further clarifications and exploitation of the "invisible" cBN phase in the buffer layer of the present sample will lead to some breakthroughs in the research on BN films.

## Acknowledgements

The authors are indebted to the assistance from Prof. Cockyane in Oxford University regarding the TEM work. This work was substantially supported by a grant from the Research Grants Council of the Hong Kong Administrative Region (Project No.: PolyU 5141/00E, account code: B-Q362) and an internal grant from the Hong Kong Polytechnic University.

## References

[1] S.F. Wong, C.W. Ong, G.K.H. Pang, K.Z. Baba-Kishi, W.M. Lau, J. Vac. Sci. Technol., A 22 (2004) 676.
[2] R. Riedel, Adv. Mater. 6 (1994) 549.
[3] S. Matsumoto, W. Zhang, Jpn. J. Appl. Phys. 39 (2000) 442.
[4] S. Matsumoto, W.J. Zhang, Diamond Relat. Mater. 10 (2001) 1868.
[5] P.B. Mirkarimi, K.F. McCarty, D. Medlin, T. Wolfer, T. Friedmann, E. Klaus, G. Cardinale, D. Howitt, J. Mater. Res. 9 (1994) 2925.
[6] M.A. Djouadi, V. Mortet, S. Khandozhko, P.Y. Jouan, G. Nouet, Surf. Coat. Technol. 142/144 (2001) 899.
[7] S. Reinke, M. Kuhr, W. Kulisch, R. Kassing, Diamond Relat. Mater. 4 (1995) 272.
[8] D. McKenzie, W. McFall, W. Sainty, C. Davis, R. Collins, Diamond Relat. Mater. 2 (1993) 970.
[9] C. Davis, Thin Solid Films 226 (1993) 30.
[10] J. Robertson, Diamond Relat. Mater. 5 (1996) 519.
[11] H. Hofsäss, H. Feldermann, R. Merk, M. Sebastian, C. Ronning, Appl. Phys., A 66 (1998) 153.
[12] W.J. Yu, W.M. Lau, S.P. Chan, Z.F. Liu, Q.Q. Zheng, Phys. Rev., B 67 (2003) 014108.
[13] X.-A. Zhao, C.W. Ong, K.F. Chan, Y.M. Ng, Y.C. Tsang, C.L. Choy, P.W. Chan, J. Vac. Sci. Technol., A 15 (1997) 2297.
[14] M. Lu, A. Bousetta, R. Sukach, A. Bensaoula, K. Walters, K. Eipers-Smith, A. Schultz, Appl. Phys. Lett. 64 (1994) 1514.
[15] Y.Y. Hui, K.W. Wong, W.M. Lau, J. Vac. Sci. Technol., A 20 (2000) 1774.
[16] E. Guiot, S. Benayoun, G. Nouet, M. Djoudi, P. Masri, M. Lambertin, Diamond Relat. Mater. 10 (2001) 1357.
[17] D.J. Kester, K.S. Ailey, R.F. Davis, Diamond Relat. Mater. 3 (1994) 323.
[18] Q. Li, L.D. Marks, Y. Lifshitz, S.T. Lee, I. Bello, Phys. Rev., B 65 (2002) 045415.
[19] Y.Y. Takamura, O. Tsuda, H. Ichinose, T. Yoshida, Phys. Rev., B 59 (1999) 10351.
[20] H.S. Yang, C. Iwamoto, T. Yoshida, J. Appl. Phys. 91 (2002) 6695.
[21] H. Hofsäss, C. Ronning, U. Griesmeier, M. Gross, Appl. Phys. Lett. 67 (1995) 46.
[22] P.B. Mirkarimi, K.F. McKarty, D.L. Medlin, Mater. Sci. Eng., R 21 (1997) 47.
[23] H. Hofsäss, C. Ronning, U. Griesmeier, M. Gross, S. Reinke, M. Kuhr, J. Zweck, R. Fischer, Nucl. Instrum. Methods B 106 (1995) 153.
[24] K.F. McCarty, D.L. Medlin, Diamond Relat. Mater. 6 (1997) 1219.
[25] G.F. Cardinal, D.L. Medlin, P.B. Mirkarimi, K.F. McCarty, D.G. Howitt, J. Vac. Sci. Technol., A 15 (1997) 196.
[26] C. Collazo-Davila, E. Bengu, C. Leslie, L.D. Marks, Appl. Phys. Lett. 72 (1997) 314.
[27] C. Collazo-Davila, E. Bengu, L.D. Marks, M. Kirk, Diamond Relat. Mater. 8 (1999) 1091.
[28] F. Banhart, M. Zwanger, H.-J. Muhr, Chem. Phys. Lett. 231 (1994) 98.
[29] Q. Li, I. Bello, L.D. Marks, Y. Lifshitz, S.T. Lee, Appl. Phys. Lett. 80 (2002) 46.
[30] C.W. Ong (email: apacwong@inet.polyu.edu.hk) and coworkers, unpublished.
[31] Q. Li, L.D. Marks, Y. Lifshitz, S.T. Lee, I. Bello, Phys. Rev., B 65 (2002) 045415.